Nucleic Acids Research, 2025, **53**, gkaf1288
https://doi.org/10.1093/nar/gkaf1288
Chemical Biology and Nucleic Acid Chemistry

Deciphering the intermolecular interactions between G-quadruplex (G4)-forming sequences

Jianjun Xia[1,†], Jiahang Zhou[1,†], Xinzhe Zhuang[1], Huangxian Ju[1], David Monchaud[2], Jonathan B. Chaires[3], Jiří Šponer[4], Jean-Louis Mergny[1,5], Jun Zhou[1,*]

[1]State Key Laboratory of Analytical Chemistry for Life Science, School of Chemistry & Chemical Engineering, Nanjing University, Nanjing 210023, China
[2]Institut de Chimie Moléculaire de l'Université de Bourgogne (ICMUB), CNRS UMR6302, Université Bourgogne Europe (UBE), Dijon 21078, France
[3]Department of Medicine, UofL Health Brown Cancer Center, University of Louisville, 505 S Hancock St, Louisville, KY 40202, United States
[4]Institute of Biophysics of the Czech Academy of Sciences, Kra´lovopolska´ 135, Brno 612 65, Czech Republic
[5]Laboratoire d'Optique et Biosciences, Ecole Polytechnique, CNRS, INSERM, Institut Polytechnique de Paris, Palaiseau 91120, France

*To whom correspondence should be addressed. Email: jun.zhou@nju.edu.cn
†The first two authors should be regarded as Joint First Authors.

Abstract

Interactions between biomolecules govern cellular biology. While protein/protein and protein/nucleic acid (DNA, RNA) interactions—and, to a lesser extent, RNA/RNA and RNA/DNA interactions—have been extensively described, a question remains as to whether and how non-canonical DNA structures might interact with each other. This is of particular interest for guanine (G)-rich sequences that can fold into G-quadruplex (G4) structures: Individual G4s are currently studied for their involvement in a myriad of cellular events (mostly pertaining to the control of gene expression), and, more recently, the interactions between two G4s have been scrutinized as being part of a novel gene expression regulatory mechanism involving chromatin remodeling through G4-mediated loop formation. The question that needs to be answered is whether G4s or their corresponding G-rich sequences are involved. We present here a series of results collected using a combination of sequences, experimental conditions, and techniques, which led us to the conclusion that G4/G4 intermolecular interactions are mostly governed by primary sequence interactions *in vitro*.

Graphical abstract

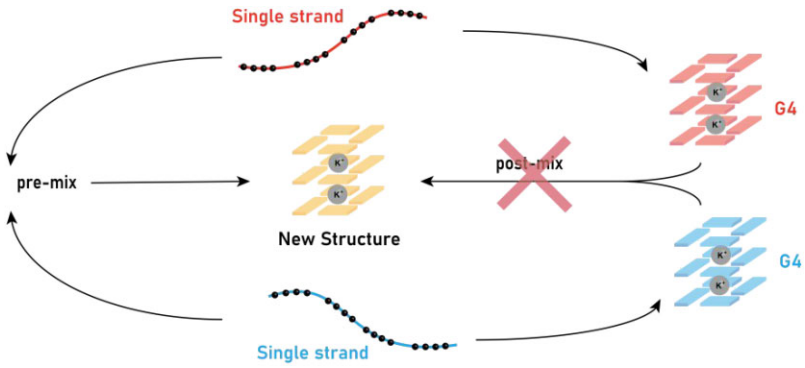

Introduction

Interactions between biomolecules (nucleic acids, proteins, saccharides, lipids, etc.) play key roles in nearly all cellular processes [1–3]. As an example, protein–protein interactions regulate cellular structure and functions, proliferation, and communication, as well as intracellular signaling pathways. Proteins can also interact with nucleic acids (DNA and RNA) to regulate both genomic and transcriptomic processes (replication, repair, transcription, post-transcriptional modifications, etc.) [4]. Interestingly, nucleic acid secondary structures play a central role in these cellular events: while this is widely accepted for RNA [5], this starts to be accepted for DNA, notably thanks to the wealth of knowledge recently accumulated about DNA G-quadruplexes (or G4s), a family of non-canonical tetraplex structures that fold from guanine (G)-rich sequences [6, 7]. In addition, while RNA/RNA and

Received: June 27, 2025. **Revised:** September 30, 2025. **Accepted:** October 21, 2025

RNA/DNA interactions are being investigated in detail (e.g. the kissing complexes for the former and the ncRNA interactome for the latter), examples of direct DNA/DNA contacts are still sparse in the literature.

Inspired by recent results showing that G4s might stimulate liquid–liquid phase separation (LLPS) thanks to weak, often long-distance intermolecular G4 interactions [8–12], we wondered whether such an interaction might take place *in vitro* during the folding process of individual G4-forming sequences. This study precisely aims at filling this gap: we investigate here whether DNA G4-forming sequences interact with each other under their unfolded (random coil) or folded (G4) conformations, and whether the topology of the G4 fold could influence these intermolecular interactions. To address these questions, we selected eight well-known G4-forming sequences [13–19] (Table 1), which encompass a diversity of G4 topologies, i.e. antiparallel G4s for TBA and 22CTA, parallel G4s for G3T, 222, and c-Myc-m, and hybrid G4s for Tel22, 4htel, and G4T2. These topologies have been established and fully characterized in routine *in vitro* experimental conditions, i.e., in the presence of 100 mM K^+ at 25°C.

These G4s were then mixed, and the resulting solutions named on the basis of mixing order and ratio. For example, the sample "TBA, Tel22-pre 2:3″ corresponds to a solution in which 2 μM TBA and 3 μM Tel22 were mixed before (PRE) adding K^+ (i.e. the two oligonucleotides were mixed, then K^+ was added to trigger the G4 folding) [16], while "TBA, Tel22-post 2:3″ corresponds to the same mixture in which the two G4 structures were folded in the presence of K^+ and then (POST) combined. The control sample "TBA, Tel22-sum 2:3″ corresponds to the algebraic addition (SUM) of the contributions of 2 μM TBA G4 on one side and 3 μM Tel22 G4 on the other side, measured separately. When applied to eight oligonucleotides, with three different topologies, at four different concentrations, with two types of mixtures (pre and post), this methodology led us to investigate the behavior of 168 different mixtures. This study, which was performed using circular dichroism, polyacrylamide gel electrophoresis, and size-exclusion chromatography, led us to draw reliable conclusions about the complex behavior of mixtures of G4-forming sequences, which turns out to be governed mostly by interactions between their unfolded rather than their folded states *in vitro*.

Materials and methods

DNA sample preparation

PAGE-purified DNA oligonucleotides were purchased from Sangon Biotech (Shanghai, China), and the concentrations of oligonucleotides were determined by UV absorbance at 260 nm. The single strands were obtained by dissolving the commercial sequences in H_2O, which were then heated at 95°C for 10 min after adding 5 mM LiOH [16]. The solution was cooled in ice and HCl was then added to adjust the pH to neutrality. The G4 samples were prepared using these single strands, then annealed in 100 mM KCl solution and placed at 4°C overnight to allow for the formation of the G4 structures. The pre-mix samples were obtained by mixing two single strands prepared at different concentration ratios with 100 mM KCl at 4°C overnight. For example, the sample TBA, G3T-pre 1:4 (corresponding to a pre-mix of 1 μM TBA and 4 μM G3T) was prepared by mixing 100 mL of 10 μM TBA single strand and 400 mL of 10 μM G3T single strand, then adding it into 500 mL of 200 mM KCl, and keeping at 4°C overnight. The post-mix samples were obtained by mixing G4 samples prepared above of the corresponding concentration (the mixing ratio) in 100 mM KCl solution at 4°C overnight. For instance, the following protocol was used for the sample TBA, G3T-post 1:4 (corresponding to a post-mix of 1 μM TBA and 4 μM G3T): Mix 100 mL of 10 μM TBA G4 and 400 mL of 10 μM G3T G4, then add it into 500 μL 100 mM KCl solution, and incubate at 4°C overnight.

Circular dichroism

CD spectra were measured with a JASCO J-1500 spectropolarimeter equipped with a Peltier accessory to control temperature. The samples were prepared as mentioned above, and the total concentration of DNA was 5 μM. The spectra were recorded from 220 to 320 nm with 10-mm path-length cuvettes at 25°C. The SUM spectra were obtained by summing the CD spectra of each individual strand at the same concentration: e.g., the control sample TBA, G3T-sum 1:4, representing the algebraic addition of the CD spectra measured individually of 1 μM TBA and 4 μM G3T in two different cuvettes. Four mixing ratios (1:4, 2:3, 3:2, and 4:1) were used to check whether the final result is influenced by the sequences, ratios, and mixing processes. The dynamic experiments were performed on the same CD spectropolarimeter mentioned above with the SFS-562T stopped-flow 2-seringue accessory. The optical path length in stopped-flow kinetic experiments was 2 mm. The dead time of the sample injection device was 100 ms, and other parameters (including monitored wavelengths, measurement time, and time interval, etc.) were fined tuned as a function of the experiments.

Size-exclusion high-performance liquid chromatography

SE-HPLC experiments were performed on an e2695 instrument (Waters), equipped with an Ultrahydrogel-250 column (7.8 × 300 mm; 6 μm hydrophilic polymethacrylate resin spherical particles, 250 Å pore size) set at 25°C. Elution was performed using 100 mM K^+ at 0.5 ml/min.

Polyacrylamide gel electrophoresis

Non-denaturing PAGE experiments were carried out on a 20% polyacrylamide gel in Tris–Borate–EDTA (TBE) buffer for 2 h at 100 V. Gels were stained with SYBR Gold (Invitrogen).

Nuclear magnetic resonance spectroscopy

^{1}H NMR (nuclear magnetic resonance) experiments were performed on a 600 MHz NMR spectrometer (Bruker) at 25°C. The total concentrations of oligonucleotides were 500 μM.

The strength index *e*

The relative change in signal intensity was identified using the strength index *e*:

$$e = \mathrm{CD}_{\mathrm{measure}} / \mathrm{CD}_{\mathrm{sum}} - 1, \quad (1)$$

where $\mathrm{CD}_{\mathrm{measure}}$ and $\mathrm{CD}_{\mathrm{sum}}$ indicate the measured and SUM results at a specific wavelength; e_{pre} and e_{post} represent the strength index of pre-mix and post-mix, respectively. $e \geq 0.05$,

Table 1. The sequences used and sample names in the study

Name	Sequence and Reference	Topology[a]
TBA	GGTTGGTGTGGTTGG[13]	Antiparallel
22CTA	AGGGCTAGGGCTAGGGCTAGGG[14]	Antiparallel
Tel22	AGGGTTAGGGTTAGGGTTAGGG[18]	Hybrid
4htel	TAGGGTTAGGGTTAGGGTTAGGGTT[19]	Hybrid
G4T2	GGGGTTGGGGTTGGGGTTGGGG	Hybrid
G3T	GGGTGGGTGGGTGGG[15]	Parallel
222	GGGTTGGGTTGGGTTGGG[16]	Parallel
c-MYC-m[b]	TGGGAGGGGTGGGAGGGTGGGG[17]	Parallel

[a]The G4 topology in 100 mM K^+ at 25°C as deduced from CD spectra and/or from the literature.
[b]This sequence derived from c-MYC can only form a parallel structure.

$e \leq -0.05$, and $-0.05 < e < 0.05$ correspond to increase, decrease, and no change in CD signal after mixing, respectively. We consider the changes in the range of −0.05 to 0.05 not to be significant.

The conformation index *r*

Topologies were identified using the conformation index *r*:

$$r = CD_{265}/\left(|CD_{265}| + CD_{295} + CD_{240}\right),$$

where CD_{240}, CD_{265}, and CD_{295} represent the CD signal at 240, 265, and 295 nm, respectively; r_{pre} and r_{post} represent the conformation index of pre-mix and post-mix conditions, respectively. These wavelengths were selected because they represent the three characteristic peaks of G4s. For instance, a CD spectrum with a positive peak at 265 nm and a negative peak at 240 nm corresponds to a parallel G4 structure. A spectrum showing positive peaks at both 295 and 240 nm, along with a negative peak at 265 nm, corresponds to an antiparallel G4 structure. It should be noted that for some sequences, there might be slight variations in these wavelengths. The sum of the 295 and 240 nm peaks allows to discriminate between parallel and hybrid G4s; the peak at 265 nm provides insights into antiparallel G4s. This is numerically expressed as *r*, with $r \geq 1$ for parallel G4s, $0 < r < 1$ for hybrid G4s, and $r \leq 0$ for antiparallel G4s. The change in topology is numerically expressed as Δr (either $\Delta r_{pre} = r_{pre} - r_{sum}$ or $\Delta r_{post} = r_{post} - r_{sum}$), with $-0.1 < \Delta r < 0.1$ corresponds to a situation in which there is no significant changes, $\Delta r > 0.1$ corresponds to an increase in parallel topology, and $\Delta r < 0.1$ corresponds to a decrease in parallel topology.

Results

To investigate the possible interactions between different G4 units, the CD technique was used as it is known to be widely responsive to G4 folding topology. Spectra were recorded in the three different situations described above, referred to as PRE, POST, and SUM hereafter. First, the CD spectra of each individual oligonucleotide collected in 100 mM K^+ (Supplementary Fig. S1) confirmed that they adopt their expected topology. When mixing two G4s (POST), the resulting CD signal was often identical to the sum of the CD signal of the two individual G4s measured separately (SUM, Supplementary Fig. S2), as expected. However, this was not always the case when recording the CD spectra of two sequences mixed before annealing (PRE, Supplementary Fig. S2): this observation implies that some G-rich sequences do indeed interact during the folding step. To characterize these interactions, we divided the sequences into four categories depending on the observed CD changes compared to SUM: (i) no significant variation (Fig. 1A); (ii) increased signal (Fig. 1B); (iii) decreased signal (Fig. 1C); or (iv) change in CD shape (Fig. 1D).

To investigate these interactions in detail, we then prepared 168 different mixtures (listed in Supplementary Fig. S2) and then analyzed them in a systematic manner. To make this analysis straightforward, we used the *e* index to describe the changes in CD intensity, defined as follows: $e = CD_{measured}/CD_{sum} - 1$, where $CD_{measured}$ and CD_{sum} indicate the measured CD signal and the SUM results at a specific wavelength, typically corresponding to the highest positive peak of CD spectra. As displayed in Fig. 1E, the e values of the PRE mix of antiparallel and hybrid structures are comprised between −0.05 and 0.05, indicating that mixing these oligonucleotides does not globally affect the final structure. In a few cases, we obtained negative values (−0.05 or lower), implying that the presence of one strand and/or G4s inhibits G4 formation (see the "Discussion" section below). The results seen in Fig. 1 can be summarized as follows: (i) The PRE mixture of parallel and antiparallel structures (Fig. 1E) had little effect on the resulting solution, with a few interesting exceptions, for instance, when mixing 222 with other sequences: large positive differences (e values >0.05) were obtained, indicating that the 222 sequence—or its G4 structure—interacts with other G4s and/or corresponding strands, facilitating their folding; (ii) the PRE mixture of parallel and hybrid structures (Fig. 1F) led to a large number of positive interactions; and (iii) all POST mixtures (Supplementary Fig. S3) do not lead to remarkable changes ($-0.05 < e < 0.05$). This first series of results thus demonstrates that mixing G-rich oligonucleotides before the annealing step (PRE mixtures) might thus have strong consequences in terms of folding, likely as a result of the interaction between the two G-strands and/or the corresponding G4 folds.

To go a step further, we introduced *r* and Δr values, which are used to illustrate the changes in G4 conformation. The *r* value is defined as follows: $r = CD_{265}/(|CD_{265}| + CD_{295} + CD_{240})$ [20, 21], where CD_{240}, CD_{265}, and CD_{295} represent the CD signal at 240, 265, and 295 nm, respectively; the Δr values are defined as follows: $\Delta r_{pre} = r_{pre} - r_{sum}$ and $\Delta r_{post} = r_{post} - r_{sum}$, where r_{pre}, r_{post}, and r_{sum} represent the *r* values of PRE and POST mixtures and SUM results, respectively. As detailed in Fig. 1G and H (and Supplementary Fig. S4), all PRE samples were very close to SUM, with the notable exception of G4T2, and no conformational changes are observed in POST samples as compared to SUM. As above, this series of results indicates that the interactions underlying these conformational changes, if any, occur during the co-folding step only (in PRE mixtures) and not after annealing (in POST

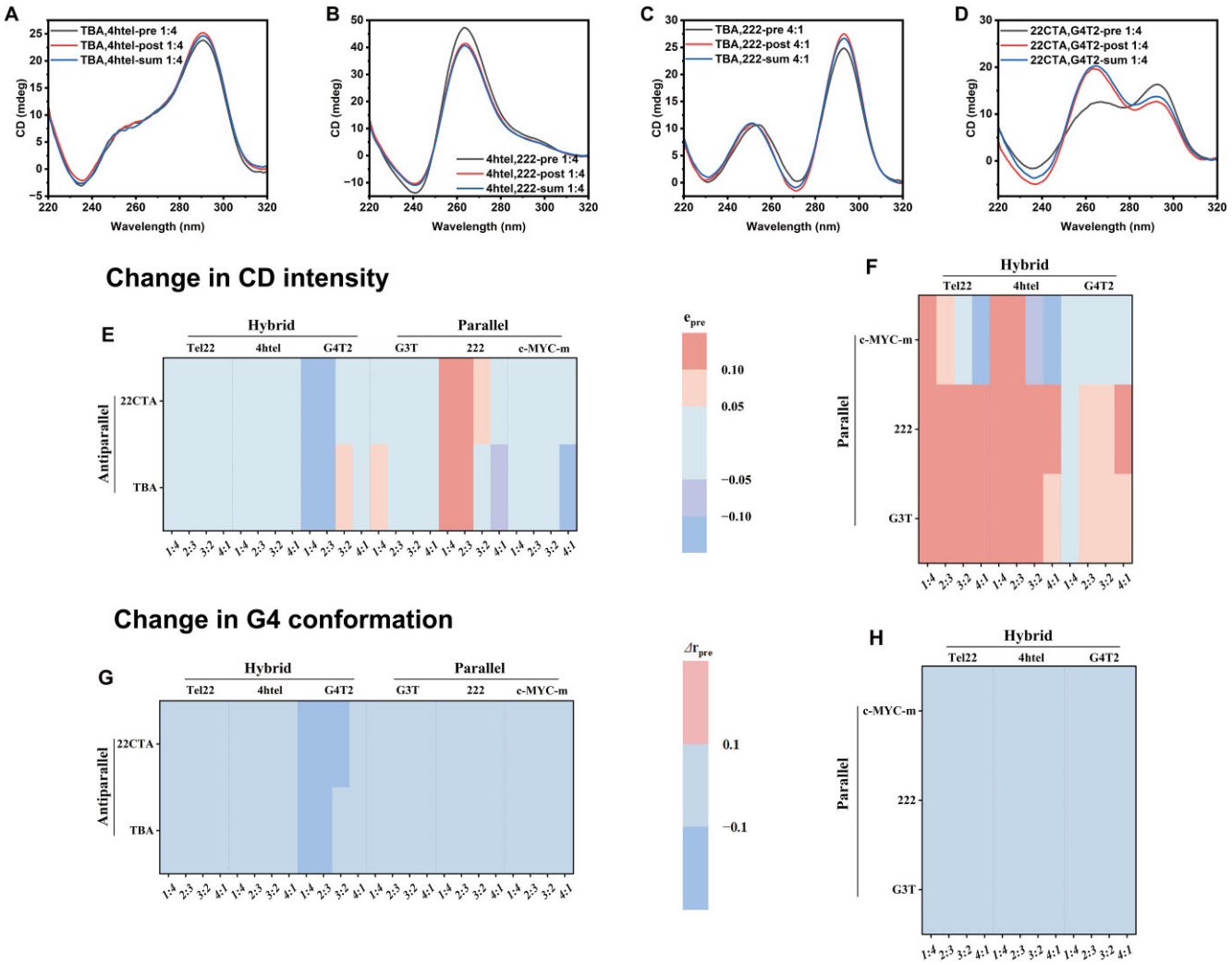

Figure 1. CD spectra of representative mixing cases (A–D) and data analysis of all the CD spectra (E–H). (**A**) Nearly no change in intensity, (**B**) increase in intensity, (**C**) decrease in intensity, and (**D**) peaks shifted. Note: all raw spectra are shown in Supplementary Fig. S2; the four panels here are representative cases of each situation. The observed discrepancy in panels (A–D) may result from different sequence composition. (E to H) Distribution of e_{pre} and Δr_{pre} values of sequences with different conformations and mixing ratios, respectively. (**E**) e_{pre} of antiparallel structure is mixed with parallel structure or hybrid structure; (**F**) e_{pre} of parallel structure mixed with hybrid structure. Panels (E) and (F) have the same scales; $e \geq 0.05$, $e \leq -0.05$, and $-0.05 < e < 0.05$ correspond to an increase, decrease, and no change in CD signal after mixing, respectively. (**G**) Δr_{pre} of antiparallel structure is mixed with parallel structure or hybrid structure. (**H**) Δr_{pre} of parallel structure is mixed with hybrid structure. Panels (G) and (H) have the same scale; $r \geq 1$, $0 < r < 1$, and $r \leq 0$ correspond to predominantly parallel, hybrid, and antiparallel topologies, respectively. $\Delta r_{pre} = r_{pre} - r_{sum}$, $\Delta r_{post} = r_{post} - r_{sum}$. $-0.1 < \Delta r < 0.1$, $\Delta r > 0.1$, and $\Delta r < 0.1$ correspond to no change in topology, increase, and decrease in parallel topology proportion, respectively.

samples). This was further confirmed by the study of the influence of the mixing ratios (from 1:4 to 4:1) on intermolecular G4 interactions (Fig. 1E–H and Supplementary Fig. S2): As above, some noticeable differences were obtained when varying the ratio of the PRE mixtures (for instance, that of 22CTA and G4T2, for which the 1:4 ratio led to a significant CD change while the 4:1 did not, suggesting that when G4T2 is predominant, 22CTA affects its folding dramatically, but not vice versa), while no differences were observed with the POST mixtures.

To go a step further in this analysis, we performed thermal unfolding experiments (Fig. 2): individual CD spectra of 22CTA and G4T2 measured at different temperatures are displayed in Fig. 2A and B, while PRE or POST mixtures at 1:4 ratio are seen in Fig. 2C and D. This approach showed that the CD signatures of the POST mixtures are in line with that of G4T2 alone [see, for instance, the signal obtained at 70°C in Fig. 2D (POST) and B (G4T2)]: this likely originates in the fact that 22CTA is unfolded at this temperature (see Fig. 2A) and therefore does not contribute to a modification of the CD signatures of the mixture. In sharp contrast, the CD signatures of the PRE mixtures are different from the individual contribution [see, for instance, the signal obtained at 70°C in Fig. 2C (PRE) and B (G4T2)], which differ not only in shape but also in intensity (14 versus 22 mdeg). These observations led us to hypothesize that PRE conditions allow for the interaction between G-strands and/or the corresponding G4 folds to form a novel structure. This was further supported by PAGE analysis, SE-HPLC analyses, and NMR data. The PAGE result shows the disappearance of the G4 bands (Fig. 3A, lanes 5 and 6) and the appearance of a new band (lane 1), while the control samples G4T2 and 222, which do not interact at 1:4

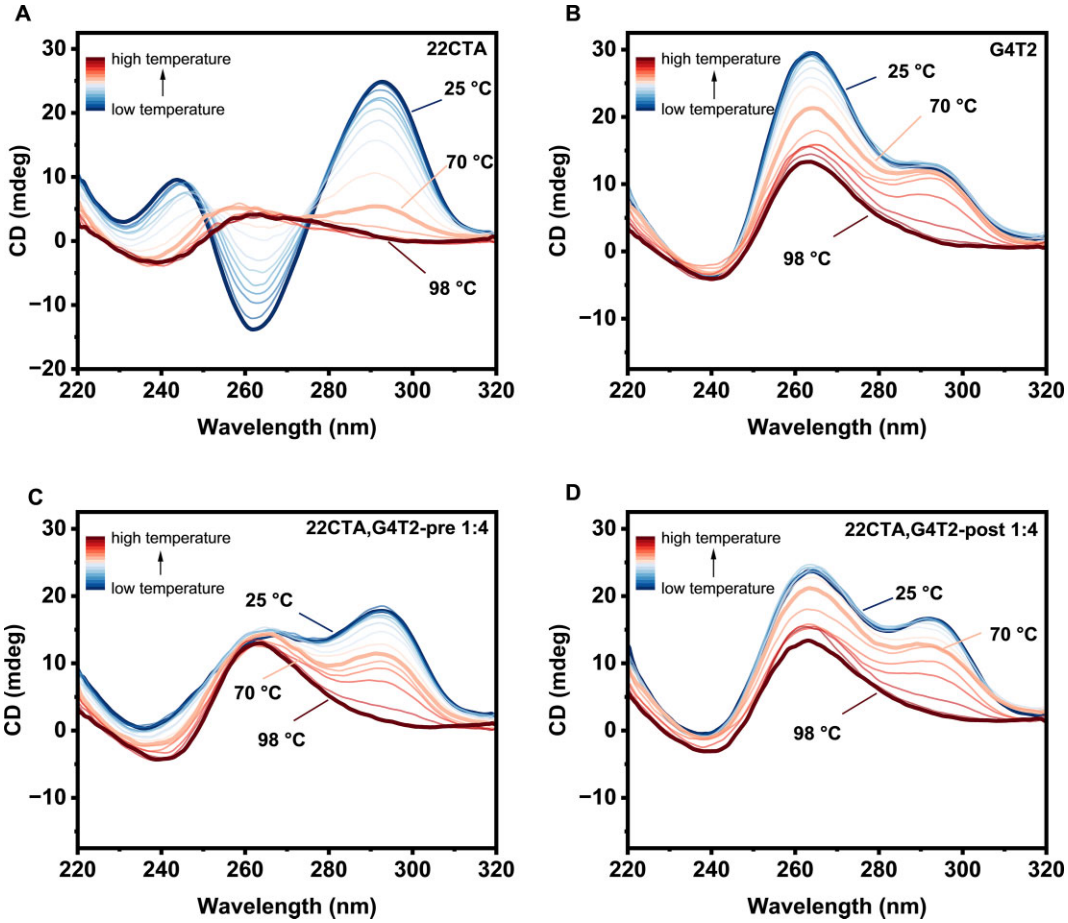

Figure 2. CD spectra of 22CTA, G4T2, and pre-mix/ post-mix of 22CTA and G4T2 at different temperatures. (**A**) 5 μM 22CTA; (**B**) 5 μM G4T2; (**C**) Pre-mix of 1 μM 22CTA and 4 μM G4T2; (**D**) Post-mix of 1 μM 22CTA and 4 μM G4T2 at 25°C (dark blue line, bold), 70°C (light orange line, bold) and 98°C (dark red line, bold). When post-mix of 22CTA and G4T2 reaches 70°C (22CTA is nearly unfolded at this temperature), its CD spectrum is nearly identical to the one of 4 μM G4T2. However, when pre-mix of 22CTA and G4T2 reaches 70°C, its CD spectrum is different from the one of 4 μM G4T2. Temperature gradient of 1°C per minute.

ratio, did not show any changes (lanes 3 and 4). This result implies that a new structure may be formed in the PRE condition. SE-HPLC analyses confirm the appearance of a new signal, whose exact nature remains to be deciphered (Fig. 3B). Finally, the ^{1}H NMR analysis (Supplementary Fig. S5) also indicates the formation of a new structure, which is different from that of the mixed monomers.

These variable temperature experiments were extended to the three other situations described in Fig. 1A–C (and Supplementary Figs S6 and S7): (i) when the CD spectra of both PRE or POST samples were identical to SUM at the corresponding temperatures; (ii) when the CD spectra of PRE samples were different from SUM at low temperatures, in line with the data shown in Fig. 1B and C, a difference that gradually decreases to eventually vanishes, with increasing temperature while the POST mixtures are similar to SUM at a given temperature; and finally (iii) when the CD spectra of the PRE samples showed a decrease in intensity as compared to SUM, which suggests an inhibition of G4 folding. The second situation is interesting: indeed, the maximal difference was observed when the least stable G4 is completely unfolded; this indicates a mutual influence (promotion or inhibition) of the two G4 structures during the folding step. To gain insights into the type of interactions that occur in PRE samples, which may involve single strands, partially folded G4s, and/or stable G4 folds, we performed stopped-flow CD kinetic experiments: we selected 222, which leads to significant variations when mixed with other sequences (see Fig. 1), in the presence of either Tel22, G3T, 22CTA, or 4htel (Fig. 4). The folding rate of sequence 222 in 100 mM K^+ is 0.13 min^{-1} at 25°C, which corresponds to rather slow folding kinetics (Supplementary Fig. S8A). Under the same conditions, the folding of 22CTA, Tel22, G3T, and 4htel is faster, with folding rates of 19.19, 2.67, 67.33, and 0.58 min^{-1}, respectively (Supplementary Fig. S8B–E), i.e., 145.9-, 20.3-, 512.0-, and 4.4-fold higher than 222, respectively (represented by $k(i)/k(222)$ values in Fig. 4E).

We therefore followed the folding of 222 alone or in the presence of the pre-folded or single-stranded versions of 22CTA, Tel22, G3T, and 4htel: as seen in Fig. 4, the addition of these four sequences to 222 affects the folding rate of 222. To quantify this effect, we used the k_{single}/k_{G4} ratio (Fig. 4E), and this analysis led to a series of conclusions: The G4s with the highest folding rates [22CTA and G3T, $k(i)/k(222) > 100$], i.e., which quite rapidly fold into their G4 structures, trigger the smallest difference [$\Delta(k_{single}/k_{G4}) = 0.02$]; Tel22, which has an intermediate folding rate [$k(i)/k(222) = 20.3$], also leads to a slightly more pronounced difference [$\Delta(k_{single}/k_{G4}) = 0.045$];

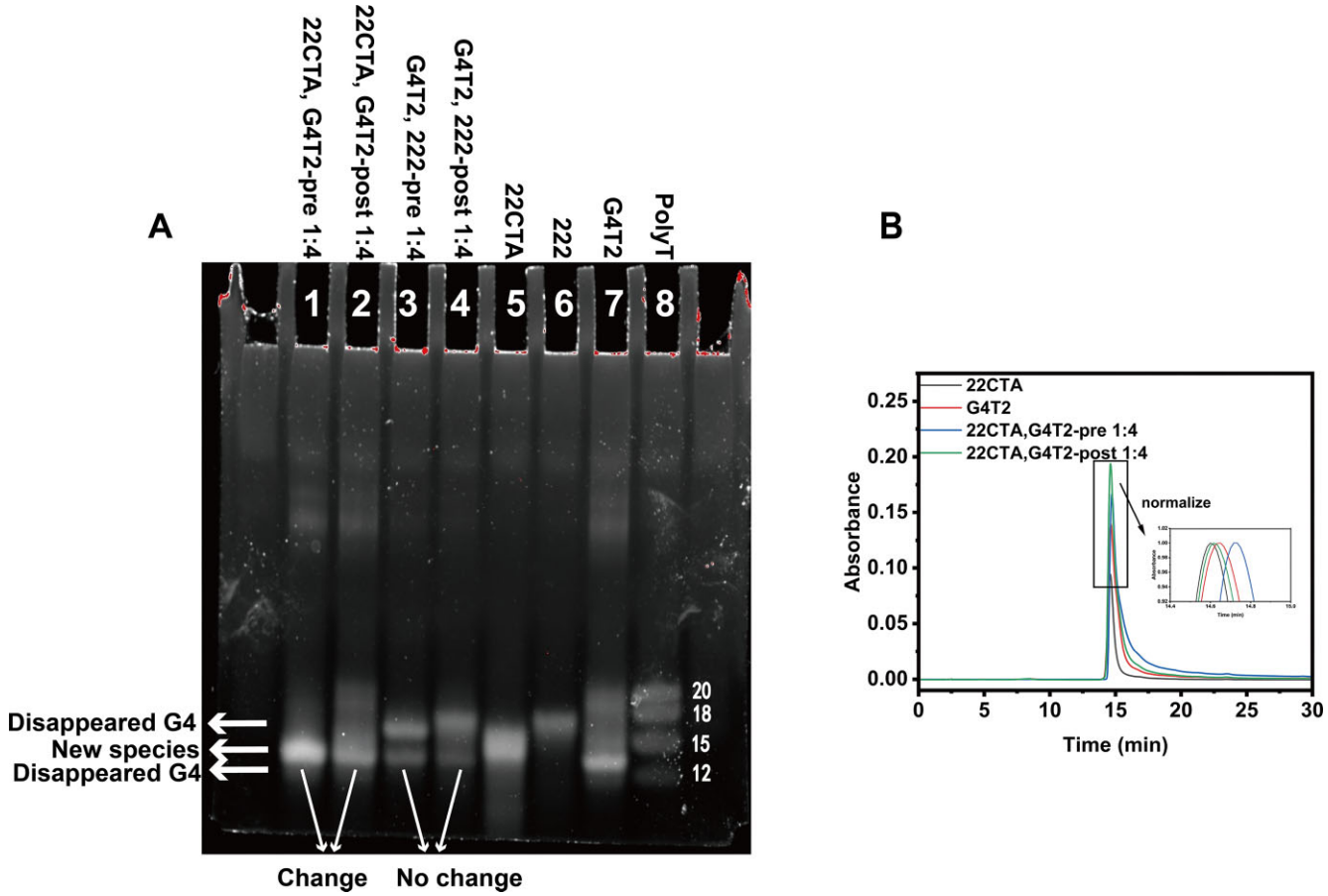

Figure 3. Analysis of the structure of 22CTA, G4T2-pre 1:4. (**A**) Electrophoregram. From left to right: (1) Pre-mix of 1 μM 22CTA and 4 μM G4T2; (2) post-mix of 1 μM 22CTA and 4 μM G4T2; (3) pre-mix of 1 μM G4T2 and 4 μM 222; (4) post-mix of 1 μM G4T2 and 4 μM 222; (5) 5 μM 22CTA; (6) 5 μM 222; (7) 5 μM G4T2; (8) markers containing different length polyT. Panels (3) and (4) were chosen as control to exhibit that there is no new structure in pre-mix/post-mix samples of 1 μM G4T2 and 4 μM 222; (**B**) SE-HPLC profiles of 10 μM 22CTA (black line), 40 μM G4T2 (red line), pre-mix of 10 μM 22CTA and 40 μM G4T2 (blue line), and post-mix of 10 μM 22CTA and 40 μM G4T2 (green line) in 100 mM KCl. It suggests that there may be new structures in 22CTA, G4T2-pre 1:4. Inset: zoom-in of the 14.4–15.0 min region of the SE-HPLC profiles.

finally, the G4 with the lowest folding rate [4htel, k(i)/k(222) = 4.4] leads to the biggest difference [$\Delta(k_{single}/k_{G4}) = 0.12$]. This provides a strong argument for supporting the hypothesis according to which the influence of Tel22, G3T, 22CTA, or 4htel on the folding of 222 primarily occurs through an interaction between the unfolded and/or partly folded sequences, and not through their G4 folds. This also explains why POST mixtures do not lead to real differences in e and ϵ indexes, because G4 are already folded and stable.

Of note, the generality of this approach was verified with other mixtures at different concentration ratios (Fig. 5 and Supplementary Fig. S9), and the collected results confirm that this trend is general (that is, not sequence-dependent).

Discussion

We aimed here at providing insights into the way G-rich DNA sequences fold into G4s in mixture with other DNA sequences, to recapitulate what may happen in cells. Our goal was to understand whether it could be reproduced *in vitro* and whether it is dictated by the G4 fold and/or the corresponding primary sequences. As an example of a corresponding biological process, a systematic analysis and experimental evaluation of a number of biologically important RNA regions involving GG motifs was recently performed, and it was shown that these motifs do not form stable intramolecular G4s but need to dimerize in order to form stable G4s [22]. Herein, the evidence we collected through three different techniques led us to conclude that the intermolecular interactions between DNA G4-forming sequences can indeed be monitored *in vitro*. It allowed us to show that the influence that one sequence can have on another sequence is primarily mediated by the interaction between their unfolded or partially folded states. These observations are interesting, as DNA and RNA G4 folding has often been seen as a purely intramolecular phenomenon in a biological context: transient or long-lasting nucleic acid interactions have long been overlooked. These inter-sequence interactions [23, 24] may provide the basis for intermolecular aggregation and LLPS, a critical phenomenon thought to be involved in the regulation of gene expression. It may also explain the length-dependent genomic instability reported for the G-rich human minisatellite CEB1, which not only depends on the potential to form intramolecular G4 structures for each individual repeat but also on the presence of multiple repeats allowing local interactions between individual G4s [25]. In this context, G4s can be considered as targets for small molecules (ligands) in order to interfere with these supramolecular regulatory mechanisms. Our results suggest that G4-forming se-

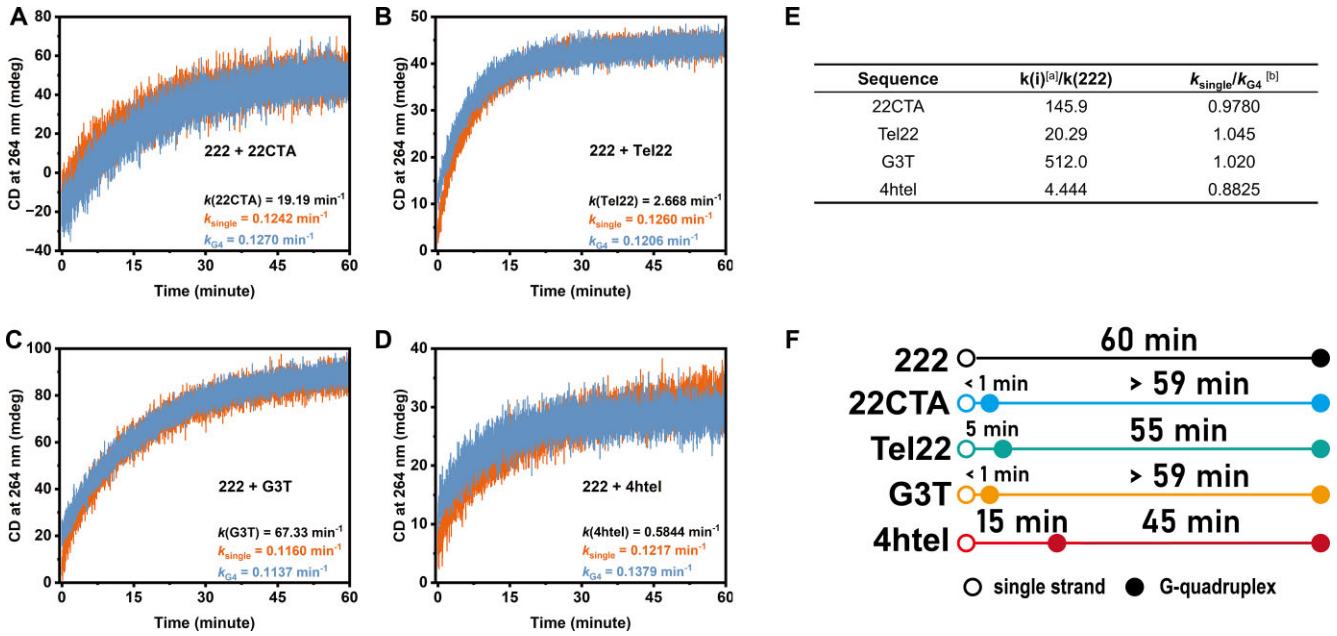

Figure 4. Time tracking curves of different samples. The time tracking curves of 5 μM 222 after the addition of 5 μM random coiled sequences (orange line, k_{single}) or G4 structures (blue line, k_{G4}) of (**A**) 22CTA, (**B**) Tel22, (**C**) G3T, and (**D**) 4htel in 100 mM K^+ at 25°C at 264 nm. The corresponding folding rate constants here demonstrate that the introduction of either random coiled sequences or folded G4 structures both changed the folding rate of 222. (**E**) Kinetics parameters. [a]Folding rate of 22CTA, Tel22, G3T, or 4htel in 100 mM K^+ at 25°C, respectively. Their data are shown in panels B–D. [b]The ratio of folding rate of 222 in the presence of single strands or G4s. The closer the value is to 1, the smaller the gap is. (**F**) Schematic of the folding times (time to reach 95% formation) of 222, 22CTA, Tel22, G3T, and 4htel.

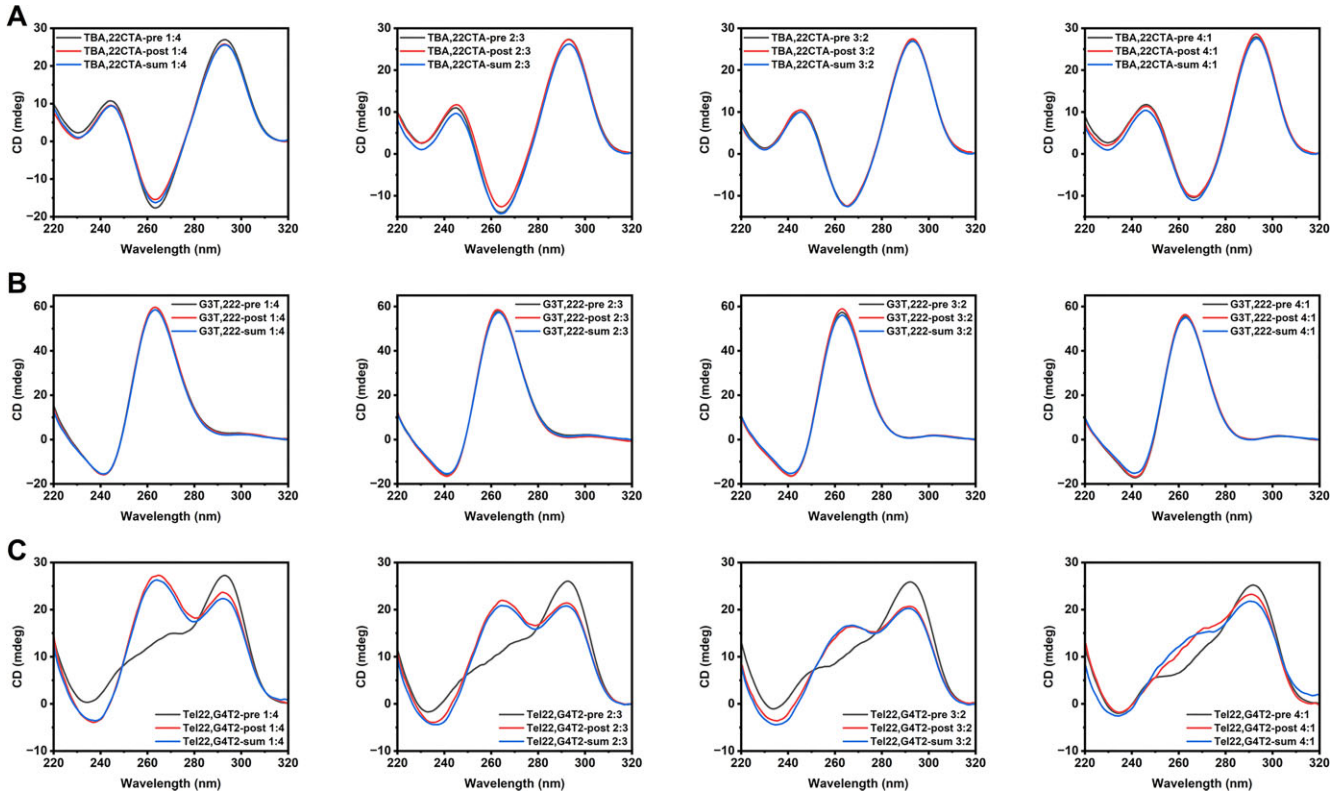

Figure 5. CD spectra of the mixture of identical conformational sequences. CD spectra of mix of (**A**) TBA, 22CTA, (**B**) G3T, 222, (**C**) Tel22, G4T2 in 100 mM KCl at 25°C (pH 7). The total concentration of DNA was 5 μM. The mixing ratios are 1:4, 2:3, 3:2, and 4:1 from left (column 1) to right (column 4), respectively. The black, red, and blue lines represent pre-mix, post-mix, and the sum of two sequences, respectively.

quences likely interact through their primary sequences, which thus has practical consequences in the aim of gaining control over this regulatory element *via* the use of *ad hoc* pharmacophores (which should not target the G4 folds but the corresponding sequences, *via* an antisense strategy for instance). Massive efforts must now be invested to assess whether these *in vitro* interactions can be reliably translated into cellular environments; our results nevertheless open a new—and very original—way to influence and harness G4-associated DNA transactions.

Acknowledgements

Author contributions: Jianjun Xia (Conceptualization [equal], Data curation [equal], Formal analysis [equal]), Jiahang Zhou (Conceptualization [equal], Data curation [equal], Formal analysis [equal]), Xinzhe Zhuang (Data curation [supporting], Formal analysis [supporting]), Huangxian Ju (Funding acquisition [supporting]), David Monchaud (Data curation [equal], Formal analysis [equal]), Jonathan (Brad) B. Chaires (Formal analysis [equal], Methodology [equal]), and Jean-Louis Mergny (Data curation [equal], Formal analysis [equal], Investigation [equal])

Supplementary data

Supplementary data is available at NAR online.

Conflict of interest

None declared.

Funding

The work was financially supported by the National Natural Science Foundation of China (22374070, 22177047), the State Key Laboratory of Analytical Chemistry for Life Science (5431ZZXM2406, SKLACLS2109, and SKLACLS2307), and the Fundamental Research Funds for the Central Universities (020514380299, 202200324, and 202200325). Funding to pay the Open Access publication charges for this article was provided by National Natural Science Foundation of China.

Data availability

Any additional data generated during the experiments are available from the corresponding author upon reasonable request.

References

1. Jena S, Dutta J, Tulsiyan KD *et al.* Noncovalent interactions in proteins and nucleic acids: beyond hydrogen bonding and π-stacking. *Chem Soc Rev* 2022;51:4261–86. https://doi.org/10.1039/D2CS00133K
2. Quintana JI, Atxabal U, Unione L *et al.* Exploring multivalent carbohydrate–protein interactions by NMR. *Chem Soc Rev* 2023;52:1591–613. https://doi.org/10.1039/D2CS00983H
3. Corradi V, Sejdiu BI, Mesa-Galloso H *et al.* Emerging diversity in lipid–protein interactions. *Chem Rev* 2019;119:5775–848. https://doi.org/10.1021/acs.chemrev.8b00451
4. Tan J, Zhao M, Wang J *et al.* Regulation of protein activity and cellular functions mediated by molecularly evolved nucleic acids. *Angew Chem Int Ed Engl* 2019;58:1621–5. https://doi.org/10.1002/anie.201809010
5. Ganser LR, Kelly ML, Herschlag D *et al.* The roles of structural dynamics in the cellular functions of RNAs. *Nat Rev Mol Cell Biol* 2019;20:474–89. https://doi.org/10.1038/s41580-019-0136-0
6. Son A, Huizar Cabral V, Huang Z *et al.* G-quadruplexes rescuing protein folding. *Proc Natl Acad Sci USA* 2023;120:e2216308120. https://doi.org/10.1073/pnas.2216308120
7. Traczyk A, Liew CW, Gill DJ *et al.* Structural basis of G-quadruplex DNA recognition by the yeast telomeric protein Rap1. *Nucleic Acids Res* 2020;48:4562–71. https://doi.org/10.1093/nar/gkaa171
8. Liu X, Xiong Y, Zhang C *et al.* G-quadruplex-induced liquid–liquid phase separation in biomimetic protocells. *J Am Chem Soc* 2021;143:11036–43. https://doi.org/10.1021/jacs.1c03627
9. Mimura M, Tomita S, Shinkai Y *et al.* Quadruplex folding promotes the condensation of linker histones and DNAs via liquid–liquid phase separation. *J Am Chem Soc* 2021;143:9849–57. https://doi.org/10.1021/jacs.1c03447
10. Wang Y, Cao K, Zong M *et al.* Mutual promotion of co-condensation of KRAS G-quadruplex and a well-folded protein HMGB1. *Nucleic Acids Res* 2023;52:288–99. https://doi.org/10.1093/nar/gkad938
11. Zhang Y, Yang M, Duncan S *et al.* G-quadruplex structures trigger RNA phase separation. *Nucleic Acids Res* 2019;47:11746–54. http://doi.org/10.1093/nar/gkz978
12. Tsuruta M, Torii T, Kohata K *et al.* Controlling liquid–liquid phase separation of G-quadruplex-forming RNAs in a sequence-specific manner. *Chem Commun* 2022;58:12931–4. https://doi.org/10.1039/D2CC04366A
13. Schultze P, Macaya RF, Feigon J. Three-dimensional solution structure of the thrombin-binding DNA aptamer d(GGTTGGTGTGGTTGG). *J Mol Biol* 1994;235:1532–47. https://doi.org/10.1006/jmbi.1994.1105
14. Lim KW, Alberti P, Guédin A *et al.* Sequence variant $(CTAGGG)_n$ in the human telomere favors a G-quadruplex structure containing a G·C·G·C tetrad. *Nucleic Acids Res* 2009;37:6239–48. https://doi.org/10.1093/nar/gkp630
15. Jing N, Hogan ME. Structure-activity of tetrad-forming oligonucleotides as a potent anti-HIV therapeutic drug. *J Biol Chem* 1998;273:34992–9. https://doi.org/10.1074/jbc.273.52.34992
16. Largy E, Marchand A, Amrane S *et al.* Quadruplex turncoats: cation-dependent folding and stability of quadruplex-DNA double switches. *J Am Chem Soc* 2016;138:2780–92. https://doi.org/10.1021/jacs.5b13130
17. Omaga CA, Fleming AM, Burrows CJ. The fifth domain in the G-quadruplex-forming sequence of the human NEIL3 promoter locks DNA folding in response to oxidative damage. *Biochemistry* 2018;57:2958–70. https://doi.org/10.1021/acs.biochem.8b00226
18. Parkinson GN, Lee MPH, Neidle S. Crystal structure of parallel quadruplexes from human telomeric DNA. *Nature* 2002;417:876–80. https://doi.org/10.1038/nature755
19. Phan AT, Kuryavyi V, Luu KN *et al.* Structure of two intramolecular G-quadruplexes formed by natural human telomere sequences in K^+ solution. *Nucleic Acids Res* 2007;35:6517–25. https://doi.org/10.1093/nar/gkm706
20. Cheng M, Cheng Y, Hao J *et al.* Loop permutation affects the topology and stability of G-quadruplexes. *Nucleic Acids Res* 2018;46:9264–75. https://doi.org/10.1093/nar/gky757
21. Del Villar-Guerra R, Trent JO, Chaires JB. G-quadruplex secondary structure obtained from circular dichroism spectroscopy. *Angew Chem Int Ed Engl* 2018;57:7171–5. https://doi.org/10.1002/anie.201709184
22. Basu P, Kejnovská I, Gajarský M *et al.* RNA G-quadruplex formation in biologically important transcribed regions: can two-tetrad intramolecular RNA quadruplexes be formed? *Nucleic Acids Res* 2024;52:13224–42. https://doi.org/10.1093/nar/gkae927

23. Liano D, Monti L, Chowdhury S *et al*. Long-range DNA interactions: inter-molecular G-quadruplexes and their potential biological relevance. *Chem Commun* 2022;58:12753–62. https://doi.org/10.1039/D2CC04872H
24. Liano D, Chowdhury S, Di Antonio M. Cockayne Syndrome B protein selectively resolves and interact with intermolecular DNA G–quadruplex structures. *J Am Chem Soc* 2021;143:20988–1002. https://doi.org/10.1021/jacs.1c10745
25. Ribeyre C, Lopes J, Boulé J-B *et al*. The yeast Pif1 helicase prevents genomic instability caused by G-quadruplex-forming CEB1 sequences in vivo. *PLoS Genet* 2009;5:e1000475. https://doi.org/10.1371/journal.pgen.1000475

Received: June 27, 2025. **Revised:** September 30, 2025. **Accepted:** October 21, 2025